



HAL
open science

Partial covering of the emission regions of Q 0528-250 by intervening H₂ clouds

V. V. Klimenko, S. A. Balashev, A. V. Ivanchik, C. Ledoux, P. Noterdaeme,
P. Petitjean, R. Srianand, D. A. Varshalovich

► To cite this version:

V. V. Klimenko, S. A. Balashev, A. V. Ivanchik, C. Ledoux, P. Noterdaeme, et al.. Partial covering of the emission regions of Q 0528-250 by intervening H₂ clouds. *Monthly Notices of the Royal Astronomical Society*, 2015, 448, pp.280-298. 10.1093/mnras/stu2672 . insu-03644738

HAL Id: insu-03644738

<https://insu.hal.science/insu-03644738>

Submitted on 25 Apr 2022

HAL is a multi-disciplinary open access archive for the deposit and dissemination of scientific research documents, whether they are published or not. The documents may come from teaching and research institutions in France or abroad, or from public or private research centers.

L'archive ouverte pluridisciplinaire **HAL**, est destinée au dépôt et à la diffusion de documents scientifiques de niveau recherche, publiés ou non, émanant des établissements d'enseignement et de recherche français ou étrangers, des laboratoires publics ou privés.

Partial covering of the emission regions of Q 0528–250 by intervening H₂ clouds

V. V. Klimenko,^{1,2★} S. A. Balashev,^{1,2} A. V. Ivanchik,^{1,2} C. Ledoux,⁴ P. Noterdaeme,³ P. Petitjean,³ R. Srianand⁵ and D. A. Varshalovich^{1,2}

¹*Ioffe Physical-Technical Institute of RAS, Polytekhnicheskaya 26, 194021 Saint Petersburg, Russia*

²*St Petersburg State Polytechnical University, Polytekhnicheskaya 29, 195251 Saint Petersburg, Russia*

³*Université Pierre et Marie-Curie, Institut d'Astrophysique de Paris, CNRS-UMR7095, 98bis boulevard Arago, F-75014 Paris, France*

⁴*European Southern Observatory, Alonso de Córdova 3107, Casilla 19001, Vitacura, Santiago 19, Chile*

⁵*Inter-University Centre for Astronomy, and Astrophysics, Post Bag 4, Ganesh Khind, Pune 411 007, India*

Accepted 2014 December 12. Received 2014 December 12; in original form 2014 October 8

ABSTRACT

We present an analysis of the molecular hydrogen absorption system at $z_{\text{abs}} = 2.811$ in the spectrum of the blazar Q 0528–250. We demonstrate that the molecular cloud does not cover the background source completely. The partial coverage reveals itself as a residual flux at the bottom of the saturated H₂ absorption lines. This amounts to about (2.22 ± 0.54) per cent of the continuum and does not depend on the wavelength. This value is small and it explains why this effect has not been detected in previous studies of this quasar spectrum. However, it is robustly detected and is significantly higher than the zero-flux level at the bottom of the saturated lines of the Ly α forest, (-0.21 ± 0.22) per cent. The presence of the residual flux could be caused by unresolved quasar multicomponents, by light scattered by dust and/or by jet–cloud interaction. The H₂ absorption system is very well described by a two-component model without the inclusion of additional components when we take partial coverage into account. The derived total column densities in the H₂ absorption components A and B are $\log N(\text{H}_2)(\text{cm}^{-2}) = 18.10 \pm 0.02$ and 17.82 ± 0.02 , respectively. HD molecules are present only in component B. Given the column density, $\log N(\text{HD}) = 13.33 \pm 0.02$, we find $N(\text{HD})/2N(\text{H}_2) = (1.48 \pm 0.10) \times 10^{-5}$, significantly lower than previous estimations. We argue that it is crucial to take into account the partial coverage effects in any analysis of H₂ bearing absorption systems, in particular when studying the physical state of the high-redshift interstellar medium.

Key words: ISM: clouds – quasars: individual: Q 0528–250 – cosmology: observations.

1 INTRODUCTION

As a result of their cosmological distances, quasars (QSOs) appear as point-like objects. Various studies have aimed to explore the detailed inner structure of quasars, which is unresolved even for low-redshift active galactic nuclei (AGNs), because of their remote distances and the subparsec scales of their emission regions. In the standard AGN paradigm, the central region is divided into an accretion disc, a dusty torus, a jet, a broad-line region (BLR) and a narrow-line region (NLR). Each of these regions contributes differently to the AGN emission spectrum.

Direct imaging of the spatial structure of AGNs is possible with current instruments that mainly probe longer scales. To date, several interferometric studies of the central engine of the brightest AGNs (e.g. Jaffe et al. 2004; López-Gonzaga et al. 2014; Tristram et al. 2014) have revealed the existence of a hot, parsec-scale disc that

is surrounded by warm dust extended in the polar direction. In the optical band, the geometry of the emission-line region is investigated by indirect methods. Reverberation mapping establishes the relationship between the size and the luminosity of the BLR and yields a typical BLR size of $R_{\text{BLR}} \sim 0.2$ pc (Kaspi et al. 2007; Chelouche & Daniel 2012) for high-redshift luminous quasars. Differential microlensing allows for a constraint on the accretion disc size $\lesssim 3 \times 10^{-3}$ pc (Blackburne et al. 2011; Jiménez-Vicente et al. 2012) and for an estimation of the size of the BLR ~ 0.1 pc (Sluse et al. 2011). The observations of gamma-ray emission constrain the size of the jet constituent to a few parsec (Abdo et al. 2010).

Another estimate of the size of the AGN emitting regions comes from constraints derived from a covering factor analysis of intervening H₂ bearing clouds, which happen to cover the background source only partially. An analysis of the partial coverage of Q 1232+082 by a molecular hydrogen absorption cloud allowed Balashev et al. (2011) to estimate the size of the C IV BLR, $R_{\text{C IV}} \sim 0.16_{-0.11}^{+0.08}$ pc.

* E-mail: slava.klimenko@gmail.com

Molecular hydrogen absorption systems, a subset of damped Ly α systems (DLAs) and sub-damped Ly α systems (sub-DLAs), reveal diffuse and translucent interstellar clouds in high-redshift intervening galaxies (Noterdaeme et al. 2008). An analysis of H₂ absorption systems allows us to examine the physical conditions of diffuse clouds in distant galaxies (Srianand et al. 2005; Noterdaeme et al. 2007). It has been shown that the gas is a part of the cold neutral medium with comparatively low kinetic temperature ($T \sim 50$ – 500 K) and high densities ($n_{\text{H}} > 10 \text{ cm}^{-3}$), and thus compact sizes ($l \lesssim 1$ pc). The comparison of 21-cm and H₂ absorptions suggests that the H₂ absorption originates from a compact gas that probably contains only a small fraction of H I measured along the line of sight (Srianand et al. 2012). These systems are important instruments for the analysis of several cosmological problems, as follows. (i) The discovery of HD/H₂ clouds at high redshift (Varshalovich et al. 2001) provides an independent way to estimate the primordial deuterium abundance (D/H) and therefore the relative baryon density of the Universe Ω_{b} , which is one of the key cosmological parameters (Balashev, Ivanchik & Varshalovich 2010; Ivanchik et al. 2010). (ii) The comparison of H₂ wavelengths observed in QSO spectra with laboratory ones (just for this quasar Q 0528–250; Varshalovich & Levshakov 1993; Cowie & Songaila 1995; Potekhin et al. 1998; Ubachs & Reinhold 2004; King et al. 2011) allows us to test the possible cosmological variation of the proton-to-electron mass ratio $\mu = m_{\text{p}}/m_{\text{e}}$. Because the decomposition of H₂ absorptions into several components is crucial for studies of the fundamental constant variability problem, we should pay attention to the partial coverage effect. It is known that when taking into account the partial coverage effects, the physical model of the absorption system differs (see Balashev et al. 2011). (iii) The interpretation of the relative populations of C I fine-structure excitation levels and CO rotational levels (Srianand, Petitjean & Ledoux 2000; Noterdaeme et al. 2011) allows us to measure the temperature $T_{\text{CMB}}(z)$ of the cosmic microwave background radiation at high redshift.

Here, we argue that it is necessary to take into account the partial coverage of quasar emission regions by a compact intervening H₂ cloud in order to derive a robust fit of the absorption lines. If this effect is not taken into account, column densities can be underestimated by a factor of up to two orders of magnitude. The first case of such an analysis has been presented by Balashev et al. (2011) for Q 1232+082. A second case of partial coverage has been detected by Albornoz Vázquez et al. (2014) for a H₂ bearing cloud towards the quasar Q 0643–504. A third case of partial coverage for the H₂ cloud at $z_{\text{abs}} = 2.811$ in the spectrum of Q 0528–2508 is presented in this study. We analyse a new spectrum and detect residual flux at the bottom of the saturated H₂ lines ($J = 0$ and $J = 1$ levels). If this flux is not taken into account, then saturated lines yield large χ^2 values and a multicomponent model is used instead (e.g. King et al. 2011).

The remainder of this paper is organized as follows. A brief description of the data is given in Section 2. The principles of partial coverage are described in Section 3. In Section 4, we present an analysis of the H₂ absorption system, accounting for partial coverage. The HD molecular lines are explored in Section 5. We discuss the results in Section 6, and we give a brief conclusion in Section 7.

2 DATA

The molecular hydrogen was identified for the first time at high redshift in the very spectrum of Q 0528–2508 (Levshakov & Varshalovich 1985). This quasar was observed many times, in par-

Table 1. Log of the observations.

No.	UT date	Programme ID	Exposure (s)	Slit (arcsec)
1	2001.02.03	66.A-0594(A)	1 × 5655	1.0
2	2001.02.04	66.A-0594(A)	2 × 5655	1.0
3	2001.02.05	66.A-0594(A)	1 × 5655	1.0
4	2001.02.07	66.A-0594(A)	1 × 5655	1.0
5	2001.02.13	66.A-0594(A)	1 × 5655	1.0
6	2001.03.13	66.A-0594(A)	1 × 5655	1.0
7	2001.03.15	66.A-0594(A)	1 × 5655	1.0
8	2001.10.17	68.A-0600(A)	1 × 3600	1.0
9	2001.10.18	68.A-0600(A)	2 × 3600	1.0
10	2002.01.08	68.A-0106(A)	2 × 3600	1.0
11	2002.01.09	68.A-0106(A)	2 × 3600	1.0
12	2002.01.10	68.A-0106(A)	2 × 3600	1.0
13	2008.11.23	082.A-0087(A)	2 × 2900	0.8–0.7
14	2008.11.25	082.A-0087(A)	1 × 2900	0.8–0.7
15	2008.12.23	082.A-0087(A)	4 × 2900	0.8–0.7
16	2009.01.25	082.A-0087(A)	1 × 2900	0.8–0.7
17	2009.01.26	082.A-0087(A)	1 × 2900	0.8–0.7
18	2009.02.26	082.A-0087(A)	1 × 2900	0.8–0.7
Total		108450		

ticular during the period between 2001 and 2009 using both spectroscopic arms of the Ultraviolet and Visual Echelle Spectrograph (UVES) of the Very Large Telescope (VLT); for a description of the instrument, see Dekker et al. (2000). The log of the observations used in our work is shown in Table 1. These observations relate to four programmes, three of which were carried out in 2001–2002: 66.A-0594(A) (PI: Molaro), 68.A-0600(A) (PI: Ledoux) and 68.A-0106(A) (PI: Petitjean). The instrument settings used during these observations were a 1-arcsec slit and 2×2 CCD pixel binning in both arms, resulting in a resolving power of $R \sim 45\,000$ in the blue and $R \sim 43\,000$ in the red. There was no ThAr lamp calibration attached to any of the exposures. An additional series of observations was performed in 2008–2009 under programme 082.A-0087(A) (PI: Ubachs). The settings for this programme were a 0.8-arcsec slit in the blue arm and a 0.7-arcsec slit in the red. The 2×2 CCD pixel binning was also used at that time. This resulted in a resolving power of $R \sim 60\,000$ in the blue and $R \sim 56\,000$ in the red. Because the goal of that programme was to set a limit on the variation of μ , ThAr lamp calibrations were also taken immediately after each observation.

The data presented in Table 1 were reduced using the UVES Common Pipeline Library (CPL) data reduction pipeline, release 4.9.5, using the optimal extraction method.¹ The inter-order background (scattered light inside the instrument) was carefully subtracted in both the flat-field frames and the science exposures. Linear spline interpolation was used to produce a two-dimensional background image, which was subsequently smoothed using an average boxcar. Fourth-order polynomials were used to find the dispersion solutions. However, the errors only reflect the calibration error at the observed wavelengths of the ThAr lines used for wavelength calibration. All the spectra were corrected for the motion of the observatory around the barycentre of the Solar system and then converted to vacuum wavelengths. These spectra were interpolated into a common wavelength array and generated the weighted-mean combined spectrum using the inverse squares of errors as weights. All the available

¹ See the UVES pipeline user manual, which is available for download at <ftp://ftp.eso.org/pub/dfs/pipelines/uves/uves-pipeline-manual-22.8.pdf>.

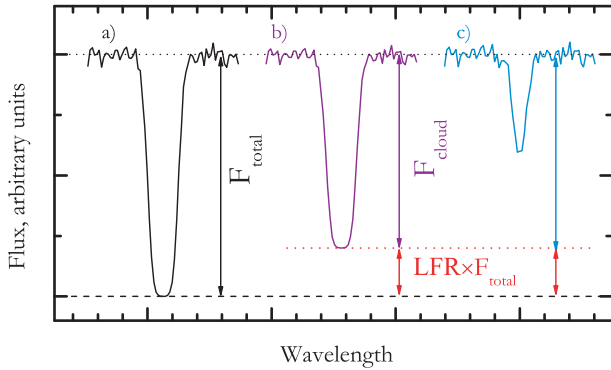


Figure 1. An illustration of the effect of partial coverage on the absorption-line profiles. The different panels show (a) a highly saturated line with total coverage, $f_c = 1$, (b) a highly saturated line with partial coverage, $f_c = 0.8$ and (c) a partially saturated line with the same partial coverage, $f_c = 0.8$. The line flux residual (LFR) is the fraction of the QSO flux that is not intercepted by the cloud. It can be easily derived from the spectral analysis in case (b), but it is not straightforward to detect in case (c).

exposures were utilized to increase the signal-to-noise ratio up to ~ 60 per pixel in the wavelength range of the H_2 absorption lines (at $z = 2.811$). As shown below, this allows us to detect and study the effect of partial coverage in detail.

3 EFFECT OF PARTIAL COVERING

Partial covering implies that only a part of the background source is covered by the absorbing cloud. Mainly, this can be a consequence of the absorbing cloud size being comparable to, or even smaller than, the projected extent of the background source.

Partial covering is readily detectable in the spectrum of a background quasar if the cores of the saturated absorption lines do not reach the zero-flux level. This indicates that a part of the radiation from the QSO passes by the cloud. The covering factor characterizing partial coverage is defined by the ratio,

$$f_c = \frac{F_{\text{cloud}}}{F_{\text{total}}}, \quad (1)$$

where F_{cloud} is the flux that passes through the absorbing gas and F_{total} is the total flux. Therefore, the measured flux in the spectrum, $F(\lambda)$, can be written as

$$F(\lambda) = [F_{\text{total}}(\lambda) - F_{\text{cloud}}(\lambda)] + F_{\text{cloud}}(\lambda) \exp[-\tau(\lambda)], \quad (2)$$

where $\tau(\lambda)$ is the optical depth of the cloud at the wavelength λ . The line flux residual (LFR) is the fraction of the QSO flux that is not covered by the cloud. These definitions are illustrated in Fig. 1. The determination of the covering factor is trivial in the case of highly saturated absorption lines (see Fig. 1, panels a and b), while for a partially saturated line (see Fig. 1, panel c) the analysis requires a more sophisticated procedure. In this case, it is necessary to use several absorption lines originating from the same levels but with different values of λf , which is the product of the oscillator strength, f , and the wavelength of the transition, λ . Such an analysis has been performed by Ivanchik et al. (2010), and more precisely by Balashev et al. (2011), for the spectrum of Q 1232+082, and by Albornoz Vázquez et al. (2014) for the spectrum of Q 0643–504. A similar situation was observed for HE0001–2340. Jones et al. (2010) have considered the possibility of partial coverage of the BLR to explain the observed $Mg\ II$ equivalent widths. In contrast to the rare situations where partial covering occurs from intervening

systems (see also Petitjean et al. 2000), partial covering is typical for absorption systems associated with quasars (e.g. Petitjean, Rauch & Carswell 1994; Rupke, Veilleux & Sanders 2005; Hamann et al. 2010; Muzahid et al. 2013).

A failure to take into account the partial coverage effect in a spectroscopic analysis can lead to a significant underestimation of the column density of an absorber. The systematic bias (of column density) can exceed several orders of magnitude for saturated lines. As an example, consider an absorption line that consists of one component and has high column density. The spectrum and the corresponding one-component model are shown in panel (a) of Fig. 2. In panels (b)–(e), the same line is presented, but part of the radiation from the background source (10 per cent for clarity) passes by a cloud. If we take into account the LFR, then the line can be properly fitted by a one-component model and we can recover the high input column density (with given accuracy) and measure the LFR value (panel e of Fig. 2). If the residual flux is not taken into account, then the one-component model – Lorentzian (b) or Gaussian (c) profiles – is not adequate, the reason being that a one-component Voigt profile cannot describe the unsaturated bottom and far wings of the line simultaneously. Using additional components, as shown in panel (d), a result with a satisfactory χ^2 is obtained. However, this solution is incorrect, because the resulting column density ($\log N = 15.8$) is much smaller than the input one ($\log N = 18.2$). To distinguish between cases (d) and (e), we propose a new method based on an analysis of several absorption lines with different oscillator strengths. The description of the method and application to the analysis of H_2 in Q 0528–250 are described in more detail later.

4 MOLECULAR HYDROGEN

Molecular hydrogen lines are detected in the spectrum of Q 0528–250 from the DLA at $z_{\text{abs}} = 2.811$. The column density of neutral hydrogen in this DLA system is $\log N(H\ I) = 21.35 \pm 0.07$ (Noterdaeme et al. 2008). The H_2 lines correspond to transitions from rotational levels up to $J = 5$. To fit the molecular hydrogen lines, the spectrum has been normalized with a continuum constructed by fitting the selected continuum regions devoid of any absorptions with spline.

4.1 Number of components

The profiles of the H_2 absorption lines have a complex structure that cannot be fitted with a single component. At least two components are clearly seen in the lines corresponding to the $J = 4$, $J = 5$ rotational levels (see Fig. 3). Since the first identification of the H_2 system in the quasar (Levshakov & Varshalovich 1985), other studies have been conducted, providing discordant results (see Table 2). Srianand et al. (2005) used a two-component model, while King et al. (2011) pointed out that a three-component model is very strongly preferred over the two-component model. King et al. (2011) used a fitting procedure where they increased the number of components in the absorption system in order to minimize the corrected Akaike information criterion² (AICC; Sugiura 1978;

²This statistical criterion allows for a choice of preferred model among several models with different numbers of fitting parameters; $AICC = \chi^2 + 2p + [2p(p + 1)/(n - p - 1)]$, where p is the number of fitting parameters and n is the number of spectral points included in an analysis.

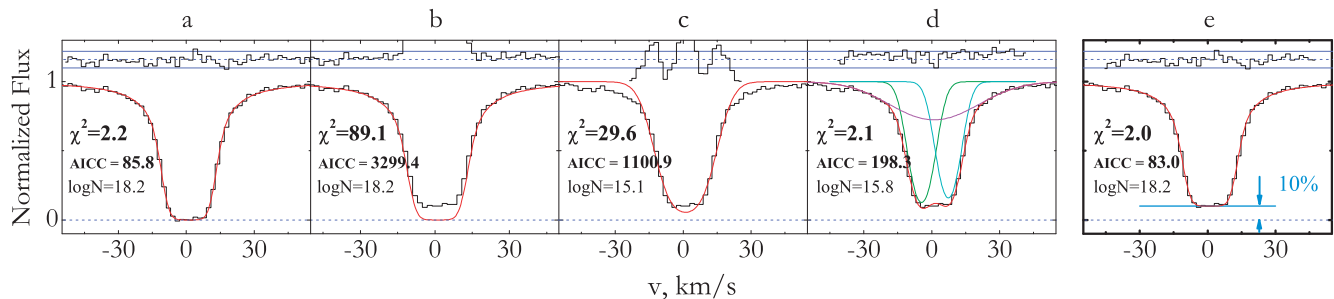


Figure 2. Panel (a) shows a single-component H₂ absorption line with $\log N = 18.2$ and $b = 4 \text{ km s}^{-1}$ and a fit by a one-component model (red line). The flux at the bottom of the line goes to zero. We add a residual flux of about 10 per cent (for clarity) to the data in panels (b)–(e). The flux at the bottom of the lines does not go to the zero level, and simultaneously the lines have Lorentzian wings. A simple one-component model cannot describe this line (cases b and c) and returns a large reduced χ^2 . However, if we add a new unresolved component to the model, the χ^2 will be significantly decreased (case d) but not the statistical criterion, the AICC (see King et al. 2011), and the returned column density will be two orders of magnitude too small.

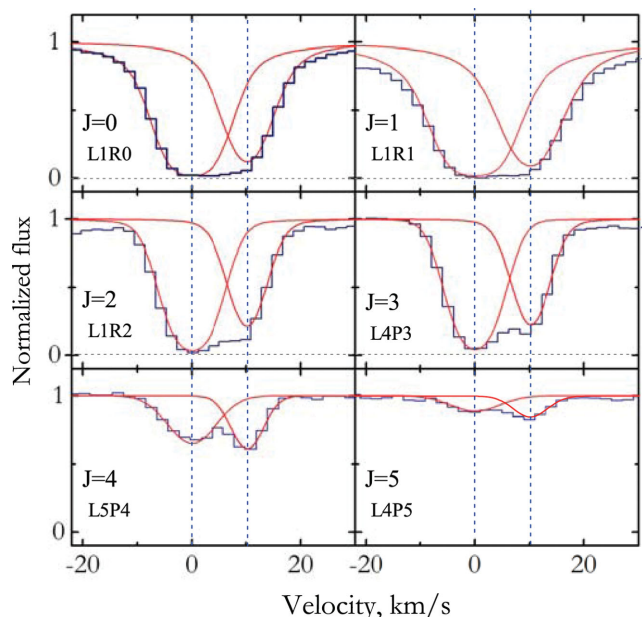


Figure 3. Examples of H₂ line profiles corresponding to the transitions from $J = 0$ –5 levels. Two components are clearly seen in the $J = 4$ and $J = 5$ lines. We have found that two components are enough to obtain a satisfying χ^2 . The origin of the velocity scale is taken at the redshift of the H₂ component, $z_A = 2.81099$.

Table 2. Results of the previous analyses of the H₂ system at $z = 2.811$ towards Q 0528–250.

Year	$\log N_{\text{tot}}$	No. of comp.	Resolution	Ref. ^a
1985	16.46 ± 0.07	1		[1]
1988	18.0	1	10 000	[2]
1998	16.77 ± 0.09	1	10 000	[3]
2005	$18.22^{+0.13}_{-0.17}$	2	40 000	[4]
2006	18.45 ± 0.02	–		[5]
2011	16.56 ± 0.02	3	45 000	[6]
2015	18.28 ± 0.02	2	45 000	This work

^a References are: [1] Levshakov & Varshalovich (1985); [2] Foltz, Chaffee & Black (1988); [3] Srianand & Petitjean (1998); [4] Srianand et al. (2005); [5] Ćirković, Damjanov & Lalović (2006); [6] King et al. (2011).

King et al. 2011). The resulting total column density differs by two orders of magnitude from Srianand et al. (2005). In that case, a criterion for choosing the preferred model is the consistent derived physical parameters of a cloud. It can be noted that by using the H₂ column density reported by King et al. (2011) (based on the three-component model) a $N(\text{HD})/2N(\text{H}_2)$ ratio is obtained that is about an order of magnitude higher than the primordial one. Meanwhile, the H₂ column density in the two-component model of Srianand et al. (2005) gives a reasonable $N(\text{HD})/2N(\text{H}_2)$ ratio, which is consistent with the typical values measured at high redshift (Balashev et al. 2010).

A very important point for the choice of a reasonable absorption profile model in the case of Q 0528–250 is the presence of Lorentzian wings in the $J = 0$, $J = 1$ line profiles (see Fig. 4). It is an indicator of the high H₂ column density of the absorption system with $\log N(\text{H}_2) > 18$, which is consistent with the result reported by Srianand et al. (2005). However, in the new spectrum of Q 0528–250, the H₂ lines with prominent Lorentzian wings have some residual flux at the bottom, which significantly differs from the zero-flux level (see Figs 4 and 5). As a consequence, the fit by Srianand et al. (2005) gives a large reduced χ^2 . It is probable that the signal-to-noise ratio in the previous spectrum was insufficient to detect the residual flux.

The current study shows that the residual flux detected at the bottom of the saturated H₂ lines in the spectrum of Q 0528–250 is the result of a partial coverage effect. In this case, the profiles of the H₂ lines can be very well fitted by a two-component model. Therefore, there is no need to increase the number of components in the H₂ profiles (as done by King et al. 2011) to explain the complex structure of lines (an example is given in Fig. 2). In the next three subsections, we provide evidence of the existence of the partial coverage in the spectrum of Q 0528–250.

4.2 Zero-flux level correction

To measure the LFR in H₂ absorption lines, we need to derive the zero-flux level in the spectrum. A non-zero flux in the core of a saturated absorption line can be the result of inaccurate determination between spectral orders of scattered light inside the instrument. The zero-flux level in the spectrum can be estimated using the saturated Ly α absorption lines, which are numerous and almost uniformly distributed over the wavelength range where H₂ absorption lines are located. Ly α lines are associated with intergalactic clouds that

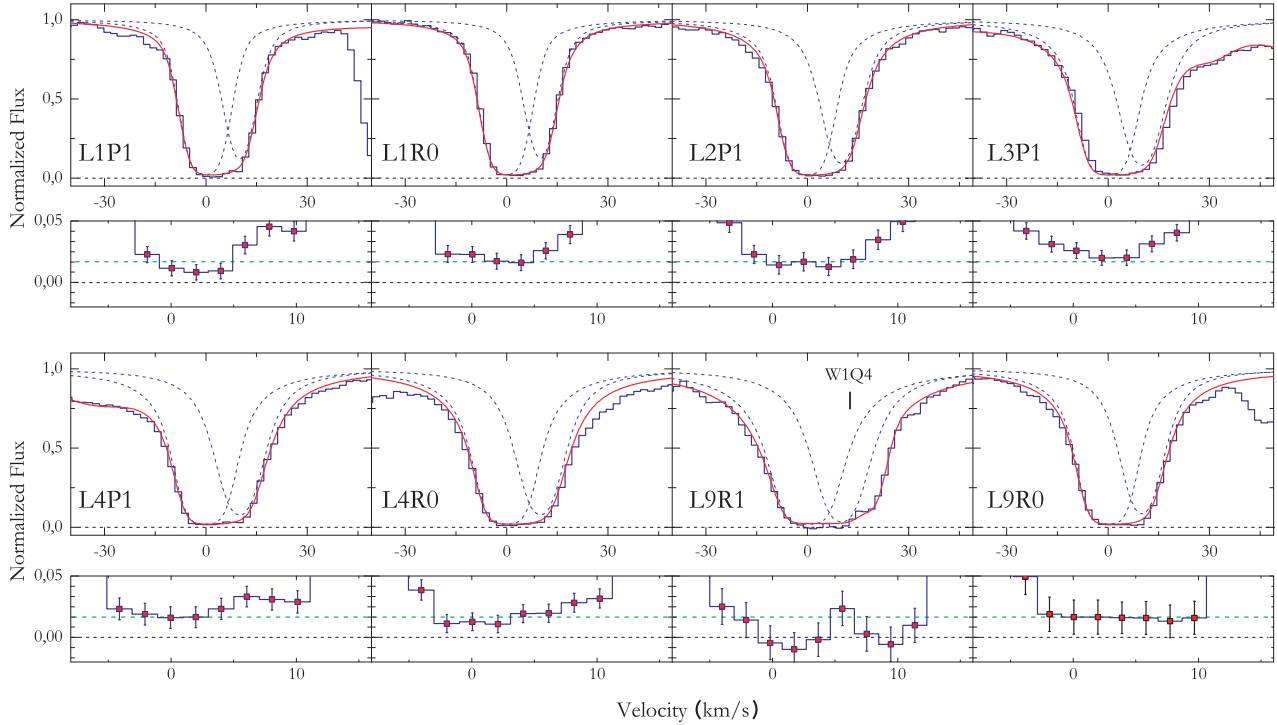


Figure 4. Some of the absorption lines of H_2 from the $J = 0, 1$ levels detected in the spectrum of Q 0528–250 and the best Voigt profile fit (red line). Two components of the absorption system are shown by blue dashed lines. Only unblended saturated lines are present. The presence of prominent Lorentzian wings of the lines indicate high H_2 column density. The additional panels show a close-up of the bottom of the corresponding lines. The dashed black horizontal line represents the zero-flux level. It is clearly seen that about 2 per cent of the LFR is present at the bottom of the saturated H_2 lines. The x-axes show the velocity offset from the centre of the H_2 component at $z = 2.81099$. In the profile of the H_2 line L9R1, some pixels at the bottom of the line are lower than the 2 per cent level, which is probably because this line is blended with $Ly\alpha$ forest absorption lines.

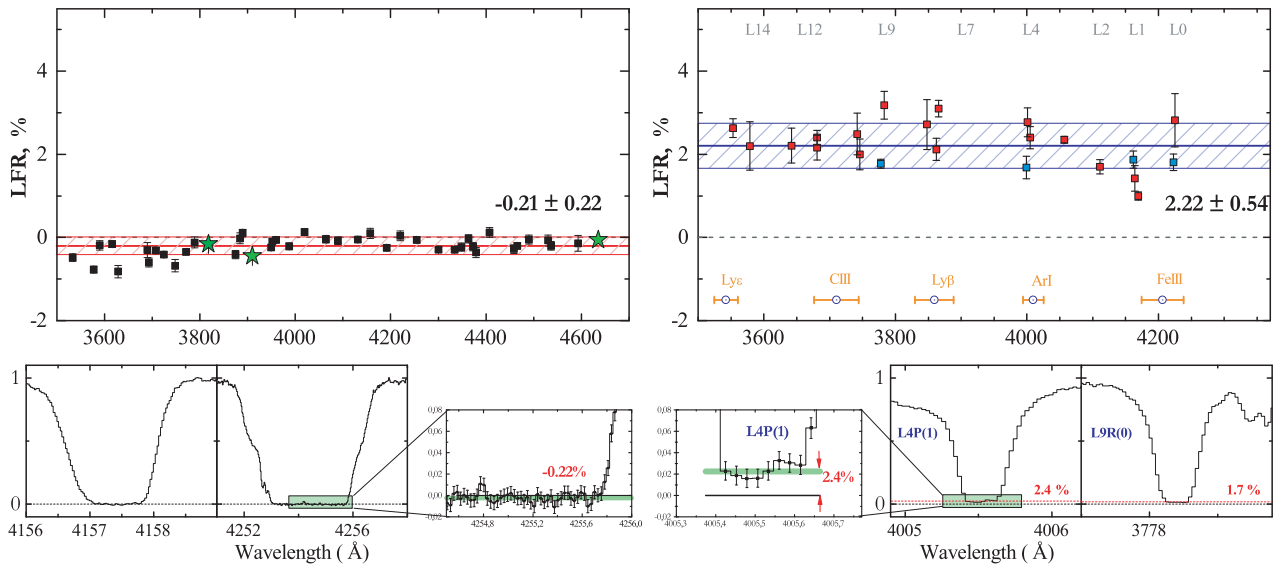


Figure 5. Top left: analysis of the zero-flux level in the spectrum of Q 0528–250. The LFRs measured at the bottom of the saturated absorption lines in the $Ly\alpha$ forest are plotted against the wavelength as filled squares. The residual fluxes are expressed in per cent of the continuum. The green stars show the LFR measured in the $Ly\beta$ and $Ly\alpha$ absorption lines of the DLA system at $z_{\text{abs}} = 2.79$ and the $Ly\alpha$ absorption from the DLA system at $z_{\text{abs}} = 2.14$. The average value of the zero-flux level is shown by the red horizontal line. The scatter in the LFR at the bottom of the lines (i.e. noise in the spectrum) is found to be at the level of 0.22 per cent. Bottom left: a few examples of saturated $Ly\alpha$ lines. The third bottom panel is the zoom of a part of the second panel. Top right: the residual fluxes at the bottom of the H_2 absorption lines from rotational levels $J = 0$ (blue) and $J = 1$ (red) are plotted against wavelengths as filled squares. The average value of the LFR in the H_2 lines is shown by the blue line. Blue circles and orange horizontal lines show the positions of QSO broad emission lines and their widths taken from Vanden Berk et al. (2001). Bottom right: a few saturated H_2 absorption lines are present. The red dashed lines show the estimated residual flux in each H_2 line. The black line indicates the zero level. The first panel shows the zoom of a part of the second panel. It can be seen that the flux in the pixels located at the bottom of the saturated H_2 lines systematically departs from zero. The shift is about 2 per cent of the continuum.

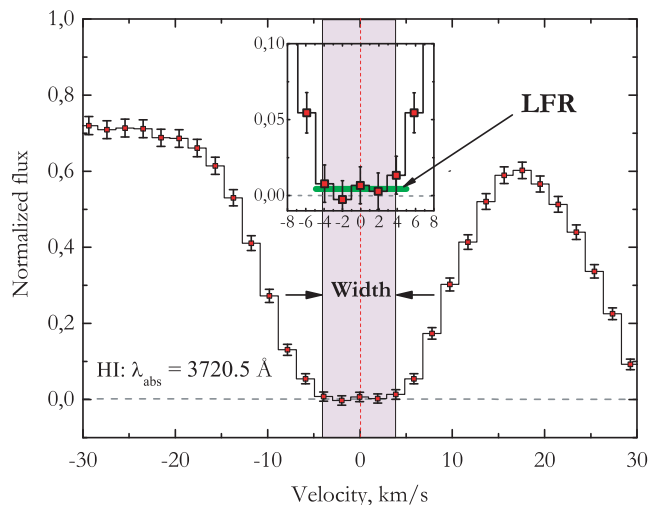


Figure 6. An illustration of the residual flux measurement procedure. To estimate the residual flux, we determine the median flux for pixels in a line profile that are in the range of $\pm 1\sigma$ from the flux at the nearest pixel to the central wavelength λ_c . This region is shown by the purple shading. We refer to the width of this region as the width of the line bottom.

are larger than several kpc, and thus it is most likely that they cover the background source completely.

Wide flat bottom lines ($\Delta\lambda > 1 \text{ \AA}$, i.e. $\delta v > 80 \text{ km s}^{-1}$) were selected, which guarantees that lines are saturated and therefore measured fluxes at the bottom of the lines (LFRs) are the real zero-flux level in the spectrum. These lines were selected in the spectral region 3500–4700 Å. To estimate the residual flux at the bottom of the line, the procedure illustrated in Fig. 6 was implemented. We selected several pixels in a line profile for which flux is within $f_c \pm 1\sigma_i$, where f_c is the flux at the centre of the line and σ_i is the error in pixel i . The residual flux was calculated as the median of the flux in the selected pixels. The width of the line bottom was estimated as the difference between the right-most and left-most selected pixels from the line centre (see Fig. 6). The top-left panel of Fig. 5 shows the LFR values obtained for the selected saturated Ly α absorption lines. The average value is found to be (-0.21 ± 0.04) per cent. The standard deviation of the points is $\sigma \simeq 0.22$ per cent. The green stars show the LFR values measured at the bottom of the Ly α and Ly β lines associated with the DLA system at $z_{\text{abs}} = 2.79$ and with the Ly α line of the second DLA system at $z_{\text{abs}} = 2.14$. These lines are the most saturated lines for the spectrum.

4.3 Partial coverage of H₂ absorption lines

To estimate the residual flux in the H₂ lines, we selected $J = 0, 1$ lines without apparent blends. The LFR was measured by the same technique as for the Ly α forest lines. The analysis found that the flux at the bottom of the lines is quite constant over a large velocity range $\delta v \simeq 10 \text{ km s}^{-1}$ (i.e. the dispersion of points is within the range of the average statistical error) that is wider than the full width half-maximum (FWHM) of the UVES (6 km s^{-1}) and is comparable with the shift between the centres of the two components. Therefore, the structure of the H₂ system has no effect on the residual flux. The comparison of the obtained residual flux in the $J = 0, 1$ H₂ lines with the level of the residual flux in the Ly α forest lines is shown in Fig. 5. The filled squares represent the residual flux in the H₂ lines versus its location in the spectrum. We have estimated the LFR at

the level 2.22 ± 0.54 per cent of the continuum, which significantly exceeds the zero-flux level.

Non-zero residual flux at the bottom of the saturated lines can also be the result of the convolution of the saturated lines with the instrumental function, or an imperfect data reduction, and/or of the blend of several unresolved unsaturated lines. First, however, the H₂ lines are wide, with widths larger than the FWHM of the UVES (6 km s^{-1} , i.e. $\sim 0.08 \text{ \AA}$). So, after convolution with the instrument function, the flux at the bottom of these lines must still go to zero. Secondly, the improper data reduction is not a viable explanation of the residual fluxes of saturated Ly α lines being consistently equal to zero. Also, we tested the dependence of residual flux on the width of the bottom of the line for H₂ and for the Ly α forest lines. This is shown in Fig. B1. Several lines in the Ly α forest were detected; these have similar widths as the H₂ lines and go to the zero level. The profiles of these lines are shown in Fig. B2.

Lastly, the residual flux cannot be a result of the composition of several unresolved unsaturated lines because the lines have Lorentzian wings.

4.3.1 The λf test

An additional test that confirms the presence of the partial coverage effect is discussed here (and illustrated in Fig. 7). Molecular hydrogen lines from $J = 0, 1$ levels have very different values of the product λf (from 0.6 for L0P1 to 36.0 for W1Q1). It is known that the flux at the bottom of an absorption line decreases exponentially when λf increases, $F \propto \exp(-\lambda f)$. The results of the calculation of this dependence for an absorption line in the spectrum with VLT resolution (FWHM = 6 km s^{-1}) are shown in Fig. 7 by dashed lines. For simplicity, the modelled line profile consists of one component. The Doppler parameter $b = 4 \text{ km s}^{-1}$ and the damping width Γ_{lm} is the same as for the H₂ line L2P1. Because the equivalent width of the line gets to the logarithmic part of the curve of growth, we do not consider the different Doppler parameters. Two dashed curves (violet and grey) are calculated for the line with column densities $\log N = 15$ and 16. The curve is shifted from right to left as the column density N increases. For a higher column density, the residual flux equals zero for a wide range of λf (because the line is saturated) and differs from zero only for small values of $\lambda f \leq 5$ (the case of an unsaturated line). In the case of a multicomponent line (i.e. the blend of two or three lines with small column density $\log N = 15$), the residual flux at the bottom of the blended line would also behave exponentially (dash-dotted curves). However, the behaviour of the residual fluxes at the bottom of the saturated H₂ lines in the spectrum of Q 0528–250 is quite different. The residual fluxes in the H₂ lines are shown by the filled blue and red squares. The squares do not follow the expected behaviour, and moreover the points scatter similarly around a median value in the whole range of λf .

Two models were applied to obtain a consistent and correct fit to the H₂ lines. Model (i) considers the best fit of a certain H₂ line (e.g. L2P1), which has a value of $\lambda f = 4.23$ and LFR = 1.7 per cent of the total flux. The line has a wide flat bottom ($\delta v \sim 10 \text{ km s}^{-1}$) and Lorentzian wings. To fit this line without partial coverage, it is necessary to use several unsaturated components in the line profile. Therefore, this model describes the line profile well. Model (ii) takes into account the partial coverage, and the line L2P1 can be fitted by the one-component model with high column density $\log N = 18.2$ and LFR = 1.7 per cent (the blue line in the right-hand

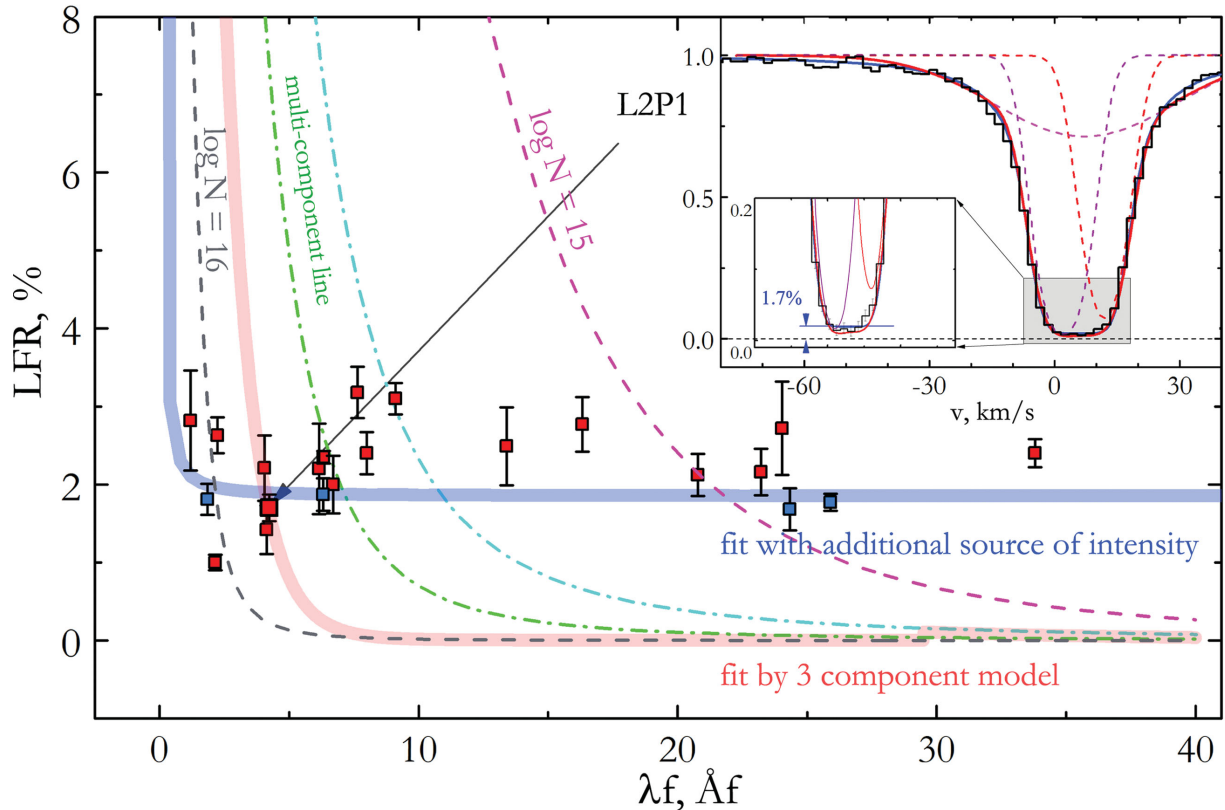


Figure 7. The residual flux at the bottom of the H₂ absorption lines is given versus the parameter λf (where f is the oscillator strength of a line). Blue and red points correspond to the H₂ lines from the $J = 0$ and $J = 1$ levels. The theoretical flux at the bottom of the one-component line with a fixed column density N and Doppler parameter b is shown by the dashed curve. The violet and grey curves correspond to column densities $\log N(\text{H}_2) = 15$ and 16 . It is seen that all points cannot be described by one curve simultaneously. The blue dash-dotted line represents the calculated residual flux at the bottom of a composite line, which consists of two components with $\log N(\text{H}_2) = 15$ for both lines and a velocity separation of $\delta v = 2 \text{ km s}^{-1}$. The green dash-dotted line presents the same model for three components with the same column densities and velocity separations of $\delta v = 2$ and 4 km s^{-1} , respectively (see text). An example is shown in the right-hand top panel. We fit a certain H₂ line (L2P1) by two models: one component with the LFR (blue line) and three components (red line). Both models give adequate fits of the line. However, the model without the LFR cannot describe the flux in all lines together, as shown by the thick red line in the graph. In contrast, all points are described by a one-component model with residual flux (see the thick blue line).

top panel). This model also describes the line profile accurately. Using only one H₂ line, we cannot determine the most probable model. However, if we consider several H₂ lines from the same J level, which cover a wide range of λf , we will be able to discriminate it. It is known that the lines from the same J level correspond to the same physical region of a molecular cloud; therefore, the lines are described by the same set of physical parameters (the column density N and Doppler parameter b). The difference between line profiles originating from the same J level is caused only by the different values of λf for the lines. Therefore, the correct model of an absorption system must describe all measurements of residual flux at the bottom of lines from a given J level simultaneously. Using the best-fitting parameters for models (i) and (ii), we have calculated the dependence of the residual flux on λf (thick red and blue curves, respectively). The thick red line cannot describe all squares in the main panel simultaneously, whereas the blue thick line can.

4.4 Voigt profile fitting

A Voigt profile fitting of the H₂ absorption lines was performed, taking into account the partial coverage. To describe a complex structure of line profiles, we have divided the total flux detected

by an observer into two parts: from a main source and from an additional one. In addition, we consider the H₂ system to be composed of two components (A and B) at redshifts $z_A = 2.81099$ and $z_B = 2.81112$. The light from the main source (~ 98 per cent of the total flux) is intercepted by the two H₂ components and does not produce any residual flux in the saturated lines. The light from the additional source that passes by the H₂ clouds is not absorbed and therefore produces a uniform residual flux in the H₂ lines. The flux in the absorption line of the two components A and B can be described as

$$F(\lambda) = (1 - f_c)F_{\text{total}} + f_c F_{\text{total}} e^{-\tau_A(\lambda)} e^{-\tau_B(\lambda)}, \quad (3)$$

where f_c (in relative units) is the covering factor for H₂ lines.

However, because the physical conditions in the A and B clouds (such as linear size, volume density, etc.) might be different, we can expect the covering factors of quasar emission regions by two H₂ clouds also to be different. In this case, the construction of the H₂ line profiles is more complicated and we present an analysis of this case below (see Appendix A). Here, it is important to note that taking into account two covering factors does not allow for a better fit to the H₂ lines (see the discussion in Appendix A).

Then, the absorption lines for each J level were described using seven fitting parameters: z_A , z_B , b_A , b_B , N_A , N_B and f_c . We used

Table 3. Column densities and Doppler parameters obtained from Voigt profile fitting of the H₂ system at $z_{\text{abs}} = 2.811$ towards Q 0528–250 after taking care of partial coverage.

System	J	z_{abs}	$\log N$ (cm ⁻²)	b (km s ⁻¹)
A	0	2.8109950(20)	17.50 ± 0.02	2.66 ± 0.05
	1	2.8109950(20)	17.93 ± 0.01	2.71 ± 0.05
	2	2.8109952(5)	16.87 ± 0.03	2.75 ± 0.03
	3	2.8109934(5)	15.97 ± 0.07	2.87 ± 0.07
	4	2.8109938(8)	14.18 ± 0.01	4.79 ± 0.11
	5	2.8109938(8)	13.58 ± 0.02	5.04 ± 0.39
B	0	2.8111240(20)	17.16 ± 0.03	1.17 ± 0.06
	1	2.8111230(20)	17.67 ± 0.02	1.14 ± 0.06
	2	2.8111235(7)	16.64 ± 0.03	1.22 ± 0.02
	3	2.8111238(6)	16.24 ± 0.06	1.25 ± 0.03
	4	2.8111231(6)	14.20 ± 0.01	1.72 ± 0.09
	5	2.8111231(6)	13.60 ± 0.02	2.38 ± 0.45

uniform values of f_c over the whole wavelength range, because the residual flux in the H₂ lines is almost independent of the wavelength (see Fig. 5). The Doppler parameter b is a function of the rotational level J . To estimate the fitting parameters, the Markov chain Monte Carlo (MCMC) method was implemented, and to speed the convergence the Affine invariant ensemble sampler by Goodman & Weare (2010) was used. The main advantage of this searching algorithm is to better explore a parameter space and to avoid using the partial derivatives of the χ^2 function, which eases a number of numerical issues. This allowed for more reliable estimates of the fitting parameters in comparison with other algorithms.

4.5 Fitting results

The H₂ absorption system at $z = 2.811$ has more than 130 absorption lines from $J = 0$ to $J = 5$ rotational levels. For the current analysis, we selected H₂ lines that are free of any obvious blends. The sample examined contains 99 lines. The best fits of the H₂ lines are shown

in Figs C1–C5, ranked following wavelength positions. The best-fitting parameters are illustrated in Table 3. The reduced χ^2 is 1.08 (the number of fitting points ~ 1500).

The H₂ absorption system is highly saturated. The total H₂ column densities are 18.10 ± 0.02 and 17.82 ± 0.02 for the A and B components, respectively. This is consistent with the presence of the Lorentzian wings in the profiles of the $J = 0$ and $J = 1$ levels. The obtained orto-to-para ratios are 2.7 ± 0.1 and 3.2 ± 0.3 for the A and B components, respectively. The corresponding kinetic temperatures of the H₂ clouds are $T_{01,A} = 141 \pm 6$ K and $T_{01,B} = 167 \pm 13$ K.

Fig. 8 shows a comparison of the H₂ excitation diagrams for our measurements and those of previous work. The left-hand panel shows the result of the analysis performed by King et al. (2011), and the right-hand panel shows the result from the present work. Because the results presented here are close to the data reported by Srianand et al. (2005), these are not shown here. We show excitation diagrams for two H₂ components at $z_A = 2.81099$ (2.811001 found by King et al. 2011) and $z_B = 2.81112$. The third H₂ component found by King et al. (2011) at $z_C = 2.8109346$ (11) is represented by the green stars. Although the ratio of the $J = 0$ and $J = 1$ levels of the third component is the same as in the other components, the excitation diagram is not physically realistic (the excitation temperatures T_{02} and T_{13} for the third component are negative). This might be the result of the incorrect model being used. It is seen that the discrepancy between our results and those of King et al. (2011) is larger only for the low J levels, where the influence of the partial coverage effect on the structure of the line profiles is significant. For high J levels, where the column densities of H₂ are less, the results agree in 1σ . To sum up, the total column density of H₂ from the measurement is 18.284 ± 0.025 , which is about two orders of magnitude larger than the value reported by King et al. (2011), 16.556 ± 0.024 .

It should be noted that the same values of N and b parameters for all transitions of one J level were used. Using the model with taking into account the partial coverage effect, we obtain the reduced

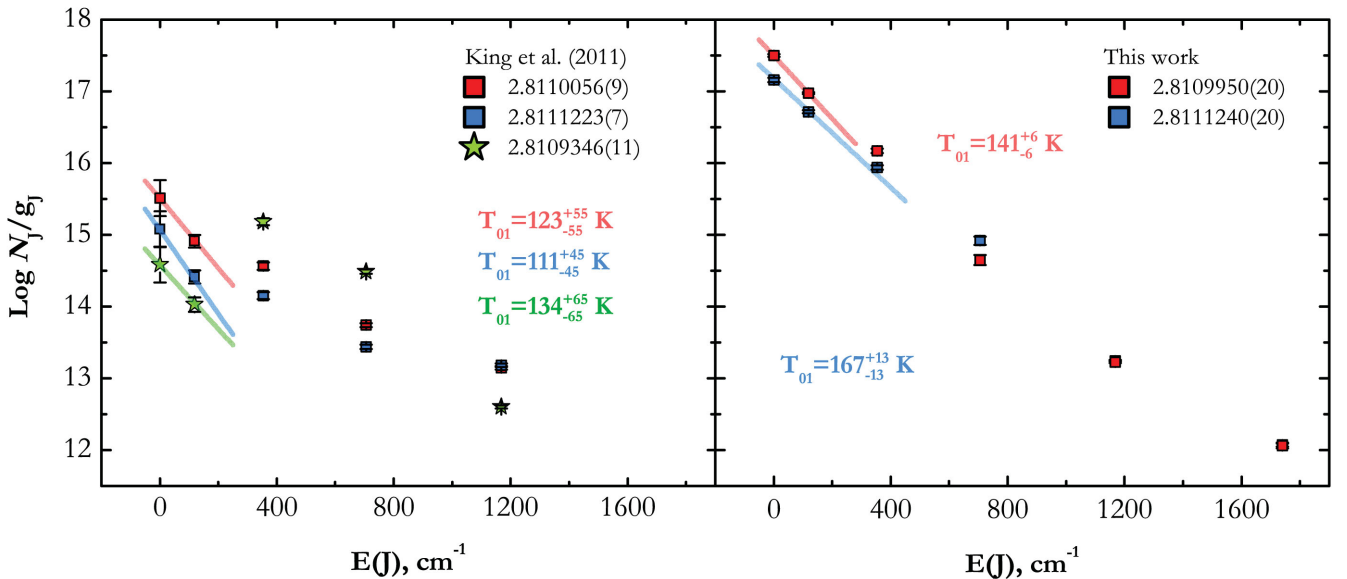


Figure 8. The excitation diagram for H₂ towards Q 0528–250. Here, N_J is the column density of the transition from the J level with g_J degeneracy. Solid lines (blue, red and green) correspond to the excitation temperature T_{01} derived from the $J = 0$ and $J = 1$ levels. The left-hand panel shows the result of the analysis performed by King et al. (2011). The excitation diagrams for different components of the H₂ system are shown by blue, red and green colours. The right-hand panel shows the results from our present work. Instead of three unsaturated components, we use two components with higher H₂ column densities.

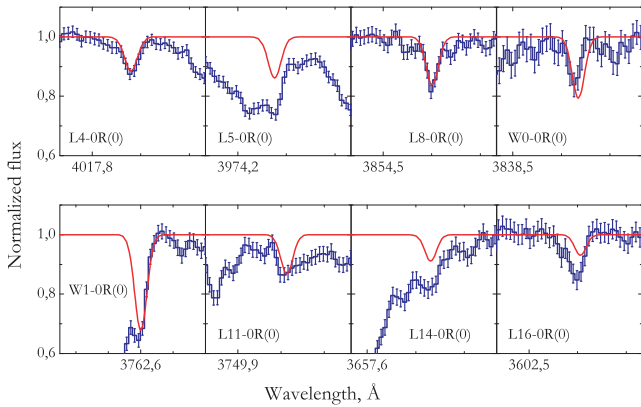


Figure 9. Line profiles of HD molecules in the absorption system at $z_{\text{abs}} = 2.811$ in the spectrum of Q 0528–250. HD lines are detected in component B only. The fit to the W0-0R(0) line is inconsistent because of the poor definition of the local continuum near the base of the Ly α line of the second DLA system at $z_{\text{abs}} = 2.14$.

Table 4. Best-fitting parameters for HD molecular lines in the spectrum of Q 0528–250.

z_{abs}	$\log N \text{ (cm}^{-2}\text{)}$	$b \text{ (km s}^{-1}\text{)}$
2.811121 ± 0.000002	13.33 ± 0.02	2.25 ± 0.53
HD/2H₂	$(1.48 \pm 0.10) \times 10^{-5}$	

$\chi^2 \simeq 1$ without an increase of the statistical errors of the spectrum. This is important, because in the previous analysis of the H₂ system in Q 0528–250 King et al. (2011) noted that without artificially increasing the statistical errors, the reduced χ^2 was $\gg 1$ (see the caption of table 6 in King et al. 2011).

The value of the residual flux in H₂ lines is fitted as an independent parameter of an analysis. The best value is 2.40 ± 0.07 per cent of the continuum, which agrees with the average value of the residual flux obtained from the analysis of $J = 0, 1$ H₂ lines (see Section 4.3).

5 HD MOLECULES

In the new spectrum (obtained by co-adding all previous and additional new observations) the molecular HD lines associated with the H₂ absorption system were detected (using improved laboratory wavelengths; Ivanov et al. 2010). The presence of HD lines in this system was first reported by King et al. (2011). The HD molecular lines are present only in the component B. Some of the HD lines are shown in Fig. 9. We have estimated the HD column density $\log N(\text{HD})_{\text{B}} = 13.33 \pm 0.02$ by analysing the two most prominent unblended absorption lines, L4-0R(0) and L8-0R(0). The results of Voigt profile fitting are shown in Table 4. Other HD lines are highly blended and cannot be used in the analysis. The obtained column density is significantly less than that required to produce self-shielding, $\log N(\text{HD}) \simeq 15$, and thus we can set only a lower limit to the isotopic ratio D/H in the cloud. Because the total column density of H₂ in the component B is $\log N(\text{H}_2) = 17.85 \pm 0.02$, we estimate $\text{D/H} \geq N(\text{HD})/2N(\text{H}_2) = (1.48 \pm 0.10) \times 10^{-5}$. The obtained HD column density is close to the result, $\log N(\text{HD}) = 13.267 \pm 0.072$, reported by King et al. (2011). However, taking into account the significantly larger H₂ column density of the component B, we have obtained a lower value of $N(\text{HD})/2N(\text{H}_2)$ than the result by King et al.

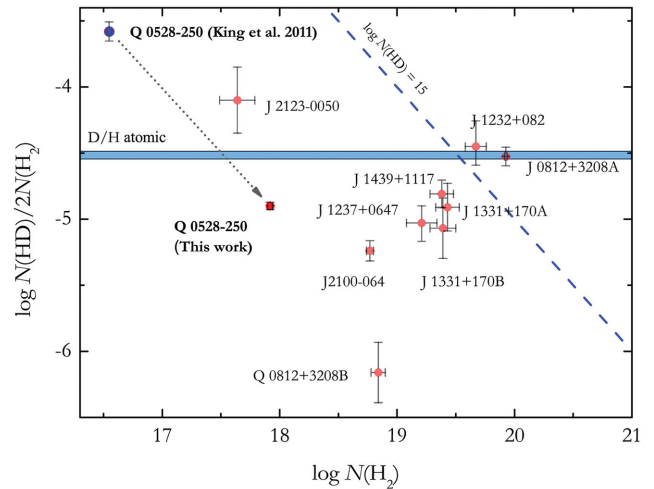


Figure 10. Measurements of $N(\text{HD})/2N(\text{H}_2)$ versus $N(\text{H}_2)$ in absorption systems at high redshift. The data are taken from Ivanchik et al. (2015). The estimates of $N(\text{HD})/2N(\text{H}_2)$ towards Q 0528–250 from this work and King et al. (2011) are shown by red and blue circles, respectively. The blue horizontal strip represents the ratio of atomic D I and H I measured in quasar spectra (Olive et al. 2012). The solid dashed line corresponds to a constant column density of HD, $\log N(\text{HD}) = 15$.

(2011). This limit is consistent with the D/H ratio obtained from the analyses of atomic species in quasar spectra (e.g. Olive et al. 2012). The comparison of this result with other $N(\text{HD})/2N(\text{H}_2)$ measurements at high redshift is shown in Fig. 10. The $N(\text{HD})/2N(\text{H}_2)$ in this system is consistent with other values and corresponds to predictions of deuterium chemistry models of diffuse ISM clouds (e.g. Balashev et al. 2010; Liszt 2014).

Note that in component B we detect HD and C I whereas in component A these species are not present, despite the higher H₂ column density of this component in comparison with component B. As for component A, we set an upper limit for HD and C I column densities, which are $\log N(\text{HD})_{\text{A}} \leq 13.1$ and $\log N(\text{C I})_{\text{A}} \leq 12.0$. The lack of HD and C I in component A might be the result of higher local UV radiation (e.g. bright young stars near cloud A). It can destroy HD and ionize C I while the H₂ molecules self-shield against the local stellar radiation because of their high column density.

6 DISCUSSION

The presence of a residual flux at the bottom of the saturated lines of the H₂ system at $z_{\text{abs}} = 2.811$ towards Q 0528–250 can be interpreted according to the arguments described in the following subsections.

6.1 Unresolved multicomponent quasars

At redshift $z \sim 2$, the internal structures in the emitting regions of quasars with transverse dimensions $\lesssim 3$ kpc are unresolved by UVES observations. For example, binary quasars with separations of the order of ~ 10 kpc (Hennawi et al. 2006; Vivek et al. 2009) might remain unresolved. Partial coverage can arise if Q 0528–250 has a complex multicomponent structure and if not all of the components are covered by the absorbing H₂ clouds.

The available Very Long Baseline Array (VLBA) image of Q 0528–250 (Kanekar et al. 2009; Srianand et al. 2012) shows

an unresolved component containing ~ 94 per cent of the total flux in the radio band (see table 6 of Srianand et al. 2012). Another ~ 6 per cent is probably emitted by a diffuse component. However, it is intriguing to note the consistency of these numbers with our findings. The spatial size of the radio emission core component is 65×380 pc (Kanekar et al. 2009), which is significantly larger than the size of the H₂ clouds. We have also looked at the images of PKS 0528–250 in 13 and 4 cm, taken as part of the National Radio Astronomy Observatories’ VLBA calibrators. The sources are unresolved even at the higher resolution achieved in these images.

6.2 Dust scattering

Scattering by dust is characterized by a narrow radiation pattern. About 90 per cent of the total flux is scattered towards the observer within less than a 5-deg opening angle (e.g. Draine 2003). The size of the scattering region can be much larger than the size of an H₂ cloud. This is why, even in the case of total coverage of the QSO by an H₂ cloud, the scattered radiation can be registered as a residual flux at the bottom of H₂ lines. The scattered flux by a dust-rich region of a DLA system can be estimated as

$$F_{\text{sc}} = F(1 - e^{-\tau_{\text{DLA}}}) \frac{\Omega_{\text{QSO}}^* \Omega_{\text{DLA}}}{\Omega_{\text{QSO}} \Omega_{\text{sc}}}, \quad (4)$$

where F is the flux that passes through an H₂ cloud and is registered by the observer, τ_{DLA} is the mean optical depth along the line of sight towards the quasar, Ω_{QSO} and Ω_{DLA} are the solid angles (measured by an observer on Earth) of the QSO emission region and the scattering region, respectively, Ω_{QSO}^* is the solid angle of the QSO emission region measured by an observer at the position of the DLA and Ω_{sc} is the solid angle in which most of the radiation is scattered by dust. Therefore, the residual flux at the bottom of the H₂ lines is $LFR = F_{\text{sc}}/F$. Assuming that a typical dimension of the scattering region is as large as 1–10 kpc, the LFR can be of the order of several per cent. This is consistent with observations. The scattered radiation can produce a non-zero residual flux for metal lines also. However it is not detected for Q 0528–250.

6.3 Jet–cloud interaction

The jet emission pointing towards us contributes to the continuum in the optical band. The extended part of the jet interacts with the external ISM and can warm up a cloud that is distant from the central source. A similar situation has been detected in the deep radio–optical–X-ray observations of the radio galaxy PKS B2152–699 by Worrall et al. (2012), who have reported the first high-resolution observations of the radio jet in the direction of an optical emission-line high ionization cloud. The *Hubble Space Telescope* image shows not only emission in the region of the high-ionized cloud – interpreted as ionized gas by Tadhunter et al. (1988) and Fosbury et al. (1998) – but also emission associated with a radio knot. The measured optical flux density of this knot at 4.97×10^{14} Hz is 2.5 ± 0.2 μJy (Worrall et al. 2012). This is strikingly similar to the value of the residual flux in the V optical band, which is 2.4 ± 0.1 μJy (using the apparent magnitude $m_V = 17.34$ of Q 0528–250; Véron-Cetty & Véron 2010). The variability of jet emission (during the period from a few days up to a month) should be high and should also induce variability of the residual flux in the H₂ line. This can be tested by further observations.

7 CONCLUSION

We have performed a detailed analysis of the H₂ system at $z_{\text{abs}} = 2.811$ towards the quasar Q 0528–250. This is a well-known system and the first detection of H₂ molecules at high redshift (Levshakov & Varshalovich 1985). The system has been analysed in a variety of research, but the results obtained are not consistent (see Table 2). The discrepancies can be explained by the presence of a residual flux at the bottom of H₂ lines, which has not been considered in previous research. We have derived the mean value of the residual flux as (2.22 ± 0.54) per cent of the continuum. This is significantly higher than the zero-flux level, (-0.21 ± 0.22) per cent, determined by analysis of the Ly α forest lines.

Taking into account the residual flux in the H₂ lines, we have obtained a consistent fit of the H₂ system using a two-component model with high column densities. The derived total column densities of components A and B are $\log N(\text{H}_2) = 18.10 \pm 0.02$ and 17.82 ± 0.02 , respectively.

We have performed the analysis of HD absorption lines detected only in component B. The estimated column density is $\log N(\text{HD}) = 13.33 \pm 0.02$ and thus we derive $N(\text{HD})/2N(\text{H}_2) = (1.48 \pm 0.13) \times 10^{-5}$. This value is consistent with other measurements of $N(\text{HD})/2N(\text{H}_2)$ in quasar spectra at high redshift and can be considered as a lower limit of the primordial deuterium abundance (Balashev et al. 2010).

Some interpretations for the presence of the residual flux are offered here: (i) a multicomponent quasar; (ii) scattering by dust; (iii) a jet–cloud interaction. We favour the latter interpretation (iii). However, new optical and radio observations of Q 0528–250 are necessary to confirm this and reject the others.

We argue that taking into account partial coverage effects is crucial for any analysis of H₂ bearing absorption systems, in particular when studying the physical state of the high-redshift ISM.

ACKNOWLEDGEMENTS

This work based on observations made with ESO Telescopes at the La Silla Paranal Observatory under programmes 66.A-0594 (PI Molaro), 68.A-0600 (PI Ledoux), 68.A-0106 (PI Petitjean) and 82.A-0087 (PI Ubachs), with the UVES spectrograph installed at the Kueyen UT2 on Cerro Paranal, Chile. VVK, SAB, AVI and DAV acknowledge support from the Dynasty foundation and by the RF President Programme (grant MK-4861.2013.2). RS and PPJ gratefully acknowledge support from the Indo-French Centre for the Promotion of Advanced Research (IFCPAR) under Project N.4304-2.

REFERENCES

- Abdo A. A. et al., 2010, *Nat*, 463, 919
 Albornoz Vásquez D., Rahmani H., Noterdaeme P., Petitjean P., Srianand R., Ledoux C., 2014, *A&A*, 562, A88
 Balashev S. A., Ivanchik A. V., Varshalovich D. A., 2010, *Astron. Lett.*, 36, 761
 Balashev S. A., Petitjean P., Ivanchik A. V., Ledoux C., Srianand R., Noterdaeme P., Varshalovich D. A., 2011, *MNRAS*, 418, 357
 Blackburne J. A., Pooley D., Rappaport S., Schechter P. L., 2011, *ApJ*, 729, 34
 Chelouche D., Daniel E., 2012, *ApJ*, 747, 62
 Čirković M. M., Damjanov I., Lalović A., 2006, *Baltic Astron.*, 15, 571
 Cowie L. L., Songaila A., 1995, *ApJ*, 453, 596

Dekker H., D'Odorico S., Kaufer A., Delabre B., Kotzłowski H., 2000, in Iye M., Moorwood A. F., eds, Proc. SPIE Conf. Ser. Vol. 4008, Optical and IR Telescope Instrumentation and Detectors. SPIE, Bellingham, WA, p. 534

Draine B. T., 2003, *ApJ*, 598, 1017

Foltz C. B., Chaffee, F. H., Jr, Black J. H., 1988, *ApJ*, 324, 267

Fosbury R. A. E., Morganti R., Wilson W., Ekers R. D., di Serego Alighieri S., Tadhunter C. N., 1998, *MNRAS*, 296, 701

Goodman J., Weare J., 2010, *Communications in Applied Mathematics and Computational Science*, 5, 65

Hamann F. W., Kanekar N., Prochaska J., Murphy M. T., Milutinovic N., Ellison S., Ubachs W., 2010, *Bulletin of the American Astronomical Society*, 41, 831 (AAS Meeting Abstracts 216, 420.03)

Hennawi J. F. et al., 2006, *AJ*, 131, 1

Ivanchik A. V., Petitjean P., Balashev S. A., Srianand R., Varshalovich D. A., Ledoux C., Noterdaeme P., 2010, *MNRAS*, 404, 1583

Ivanchik A. V., Balashev S. A., Varshalovich D. A., Klimenko V. V., 2015, *Astron. Rep.*, 59, 100

Ivanov T. I., Dickenson G. D., Roudjane M., de Olivera N., Joyeux D., Nahon L., Tchchang-Brillet W.-Ü. L., Ubachs W., 2010, *Molecular Physics*, 104, 771

Jaffe W. et al., 2004, *Nat*, 429, 47

Jiménez-Vicente J., Mediavilla E., Muñoz J. A., Kochanek C. S., 2012, *ApJ*, 751, 106

Jones T. M., Misawa T., Charlton J. C., Mshar A. C., Ferland G. J., 2010, *ApJ*, 715, 1497

Kanekar N., Lane W. M., Momjian E., Briggs F. H., Chengalur J. N., 2009, *MNRAS*, 394, L61

Kaspi S., Brandt W. N., Maoz D., Netzer H., Schneider D. P., Shemmer O., 2007, *ApJ*, 659, 997

King J. A., Murphy M. T., Ubachs W., Webb J. K., 2011, *MNRAS*, 417, 3010

Levshakov S. A., Varshalovich D. A., 1985, *MNRAS*, 212, 517

Liszt H. S., 2014, *ApJ*, in press ([arXiv:1411.5055](https://arxiv.org/abs/1411.5055))

López-Gonzaga N., Jaffe W., Burtscher L., Tristram K. R. W., Meisenheimer K., 2014, *A&A*, 565, A71

Muzahid S., Srianand R., Arav N., Savage B. D., Narayanan A., 2013, *MNRAS*, 431, 2885

Noterdaeme P., Petitjean P., Srianand R., Ledoux C., Le Petit F., 2007, *A&A*, 469, 425

Noterdaeme P., Ledoux C., Petitjean P., Srianand R., 2008, *A&A*, 481, 327

Noterdaeme P., Petitjean P., Srianand R., Ledoux C., López S., 2011, *A&A*, 526, L7

Olive K. A., Petitjean P., Vangioni E., Silk J., 2012, *MNRAS*, 426, 1427

Petitjean P., Rauch M., Carswell R. F., 1994, *A&A*, 291, 29

Petitjean P., Aracil B., Srianand R., Ibata R., 2000, *A&A*, 359, 457

Potekhin A. Y., Ivanchik A. V., Varshalovich D. A., Lanzetta K. M., Baldwin J. A., Williger G. M., Carswell R. F., 1998, *ApJ*, 505, 523

Rahmani H. et al., 2013, *MNRAS*, 435, 861

Rupke D. S., Veilleux S., Sanders D. B., 2005, *ApJS*, 160, 87

Sluse D. et al., 2011, *A&A*, 528, A100

Srianand R., Petitjean P., 1998, *A&A*, 335, 33

Srianand R., Petitjean P., Ledoux C., 2000, *Nat*, 408, 931

Srianand R., Petitjean P., Ledoux C., Ferland G., Shaw G., 2005, *MNRAS*, 362, 549

Srianand R., Gupta N., Petitjean P., Noterdaeme P., Ledoux C., Salter C. J., Saikia D. J., 2012, *MNRAS*, 421, 651

Sugiura N., 1978, *Communications in Statistics – Theory and Methods*, 7, 13

Tadhunter C. N., Fosbury R. A. E., di Serego Alighieri S., Bland J., Danziger I. J., Goss W. M., McAdam W. B., Snijders M. A. J., 1988, *MNRAS*, 235, 403

Tristram K. R. W., Burtscher L., Jaffe W., Meisenheimer K., Höing S. F., Kishimoto M., Schartmann M., Weigelt G., 2014, *A&A*, 563, A82

Ubachs W., Reinhold E., 2004, *Phys. Rev. Lett.*, 92, 101302

Vanden Berk D. E. et al., 2001, *AJ*, 122, 549

Varshalovich D. A., Levshakov S. A., 1993, *Soviet Journal of Experimental and Theoretical Physics Letters*, 58, 237

Varshalovich D. A., Ivanchik A. V., Petitjean P., Srianand R., Ledoux C., 2001, *Astron. Lett.*, 27, 683

Véron-Cetty M.-P., Véron P., 2010, *A&A*, 518, A10

Vivek M., Srianand R., Noterdaeme P., Mohan V., Kuriakosde V. C., 2009, *MNRAS*, 400, L6

Whitmore J. B., Murphy M. T., Griest K., 2010, *ApJ*, 723, 89

Worrall D. M., Birkinshaw M., Young A. J., Momtahan K., Fosbury R. A. E., Morganti R., Tadhunter C. N., Verdoes Kleijn G., 2012, *MNRAS*, 424, 1346

APPENDIX A: TEST OF A MODEL WITH TWO ADDITIONAL SOURCES OF RESIDUAL FLUX

In this section, we consider a model of the absorption system, where the projected area over the illuminating source is different for components A and B. In this case, the structure of the H₂ line profiles is more complicated. To describe a flux detected by an observer, we divide a quasar emission region into three parts: the main source and two additional sources. The main source is covered by both H₂ clouds and does not produce residual flux in the absorption lines. Additional sources can produce residual flux in two different ways (depending on the geometry of the additional sources and the H₂ clouds; see Fig. A1), as follows.

(i) One source (not covered by both clouds) produces the same residual flux in the profiles of both H₂ systems. Another source is covered by one cloud and produces residual flux only in the profile of the second system:

$$F(\lambda) = mF_{\text{total}}(\lambda) + nF_{\text{total}}(\lambda)e^{-\tau_A(\lambda)} + (1 - m - n)F_{\text{total}}(\lambda)e^{-\tau_A(\lambda) - \tau_B(\lambda)}. \quad (\text{A1})$$

(ii) Each source produces the residual flux only for one system:

$$F(\lambda) = mF_{\text{total}}(\lambda)e^{-\tau_B(\lambda)} + nF_{\text{total}}(\lambda)e^{-\tau_A(\lambda)} + (1 - m - n)F_{\text{total}}(\lambda)e^{-\tau_A(\lambda) - \tau_B(\lambda)}. \quad (\text{A2})$$

Here, m and n indicate the intensities of the additional sources in relative units. The results of the Voigt profile fitting of H₂ lines using different models of the H₂ system are presented in Table A1. The values of AICC for models A and B are significantly lower than for model C, which could indicate the presence of one additional source of quasar radiation uncovered by both H₂ clouds. Taking into account the second additional source (for system B) does not dramatically change the AICC value and we have not found strong evidence for choosing a preferred model. Therefore, we use the simplest model (with one additional source) to analyse the H₂ system.



Figure A1. An illustration of the possible explanation of the partial coverage effect for a case with independent sources of radiation (see text for details).

Table A1. Comparison of the models of the H₂ system with a different number of additional sources of radiation. Model A indicates the model with one additional source (used in this work) and models B and C correspond to models (i) and (ii) described earlier in Appendix refmodel2. Here, p is the number of fitting parameters, AICC is the Akaike information criterion (see Section 4.1) and m and n indicate the intensity of additional sources relative to the total flux of a quasar.

Model	p	AICC	Δ AICC	$m, 10^{-2}$	$n, 10^{-2}$
A	31	3096.0	12.9	2.4 ± 0.1	0
B	32	3083.1	0	2.0 ± 0.1	4.0 ± 0.3
C	32	3331.1	248.0	2.4 ± 0.1	7.6 ± 0.3

APPENDIX B: EXPOSURE SHIFT ANALYSIS

Because the final spectrum of Q 0528–250 is the co-addition of 27 exposures, the non-zero residual flux at the bottom of saturated absorption lines (such as H₂ lines) could arise due to the average velocity shifts between exposures, up to 500 m s⁻¹, and/or intra-order velocity distortions, up to 1500 m s⁻¹ (e.g. Whitmore, Murphy & Griest 2010; Rahmani et al. 2013). Also, such a small LFR could be the result of the dramatic shift of even one exposure (e.g. Rahmani et al. 2013). In that case, all narrow saturated absorption lines would have the same non-zero residual fluxes, whereas the

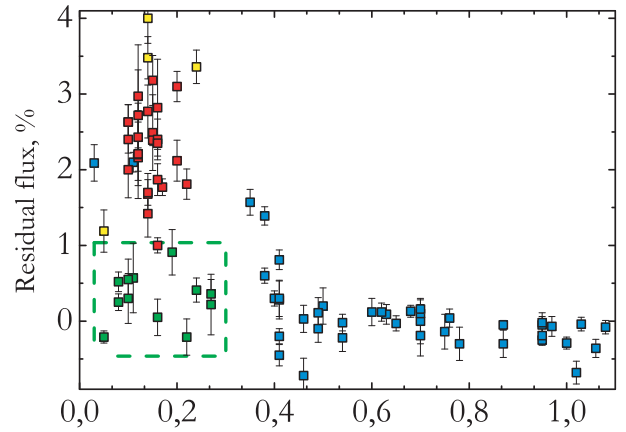


Figure B1. Dependence of residual fluxes at the bottom of lines on the widths of the bottom of lines. Blue points correspond to all saturated Ly α forest lines with $\lambda > 3500$ Å, and reached the zero-flux level within 5 per cent. The yellow points mark Ly α absorbers, which have also Ly β absorption lines in the spectrum. The red points represent the residual fluxes in H₂ lines. Among the Ly α forest lines, there are lines with LFR < 1 per cent and the width of the bottom < 0.3 Å. We have marked these in green. The existence of such lines indicates that the residual fluxes in H₂ lines are not the instrumental effect (see text for details).

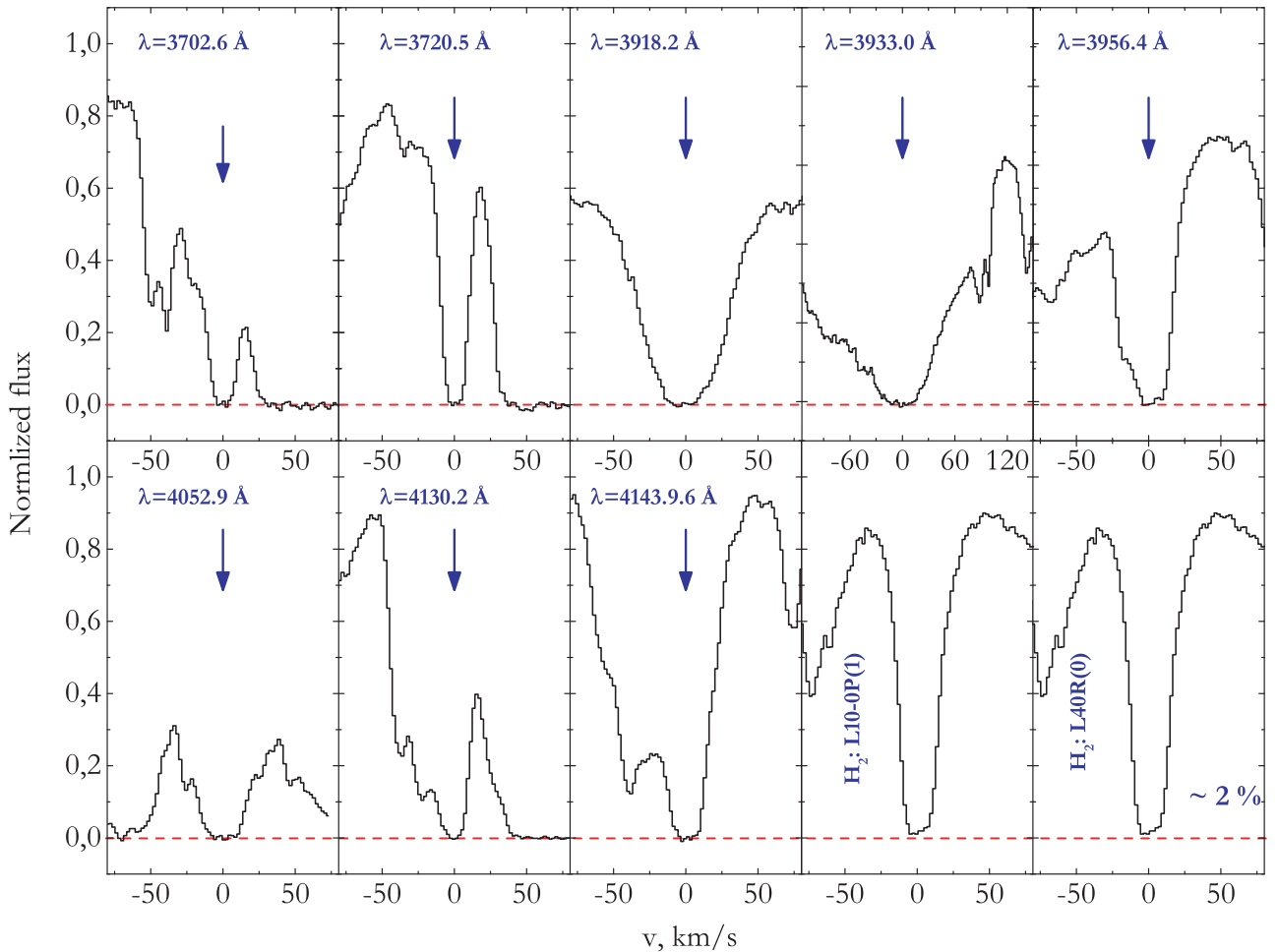


Figure B2. Profiles of the Ly α forest lines corresponding to the green filled squares in Fig. B1. For comparison, we also show two H₂ lines, L10-0P(1) and L4-0R(0), in the two bottom-right panels. The red horizontal line represents the zero-flux level.

APPENDIX C: BEST FIT OF H₂ LINES

Here we present the figures of the best fit of the H₂ lines.

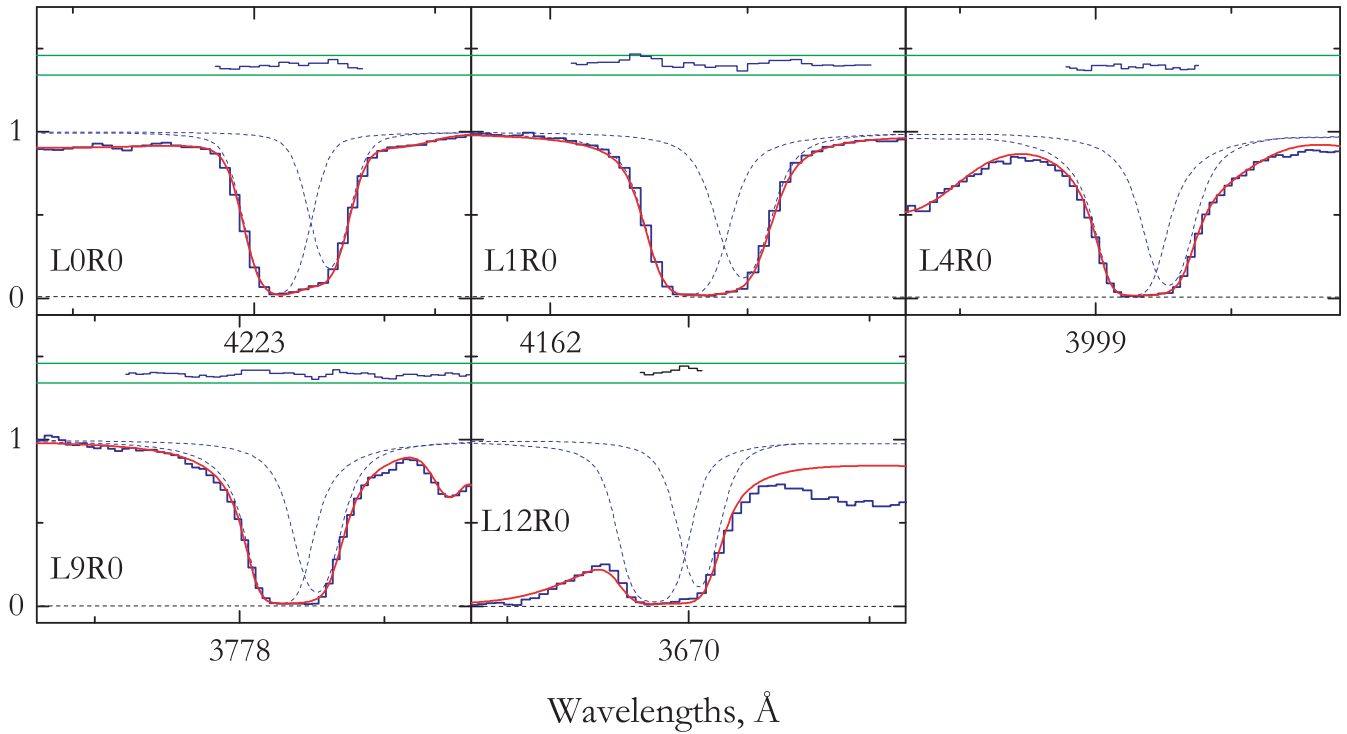


Figure C1. Best fit of the H₂ absorption lines from the $J=0$ level at $z_{\text{abs}} = 2.811$ towards Q 0528–250 (after incorporating the correction for partial coverage). Two components of the absorption system are shown by blue dashed lines. The residuals between the fit and the data are shown in the top of each panel by the dark blue line. Horizontal green lines represent $\pm 3\sigma$ levels.

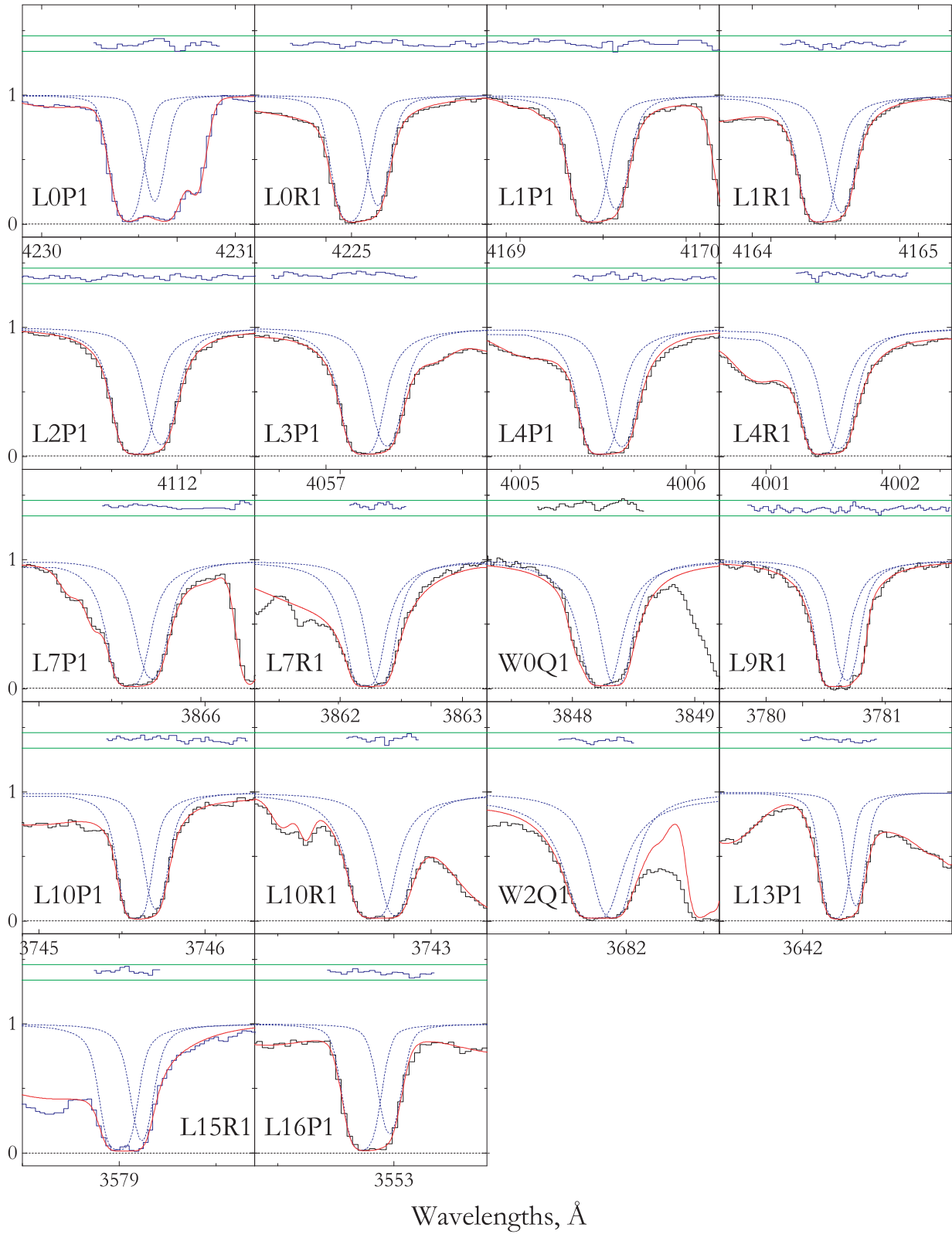


Figure C2. Best fit of the H₂ absorption lines from the $J = 1$ level at $z_{\text{abs}} = 2.811$ towards Q 0528–250. Colours and lines are the same as in Fig. C1.

Downloaded from https://academic.oup.com/mnras/article/448/1/280/990571 by CNRS - ISTO user on 25 April 2022

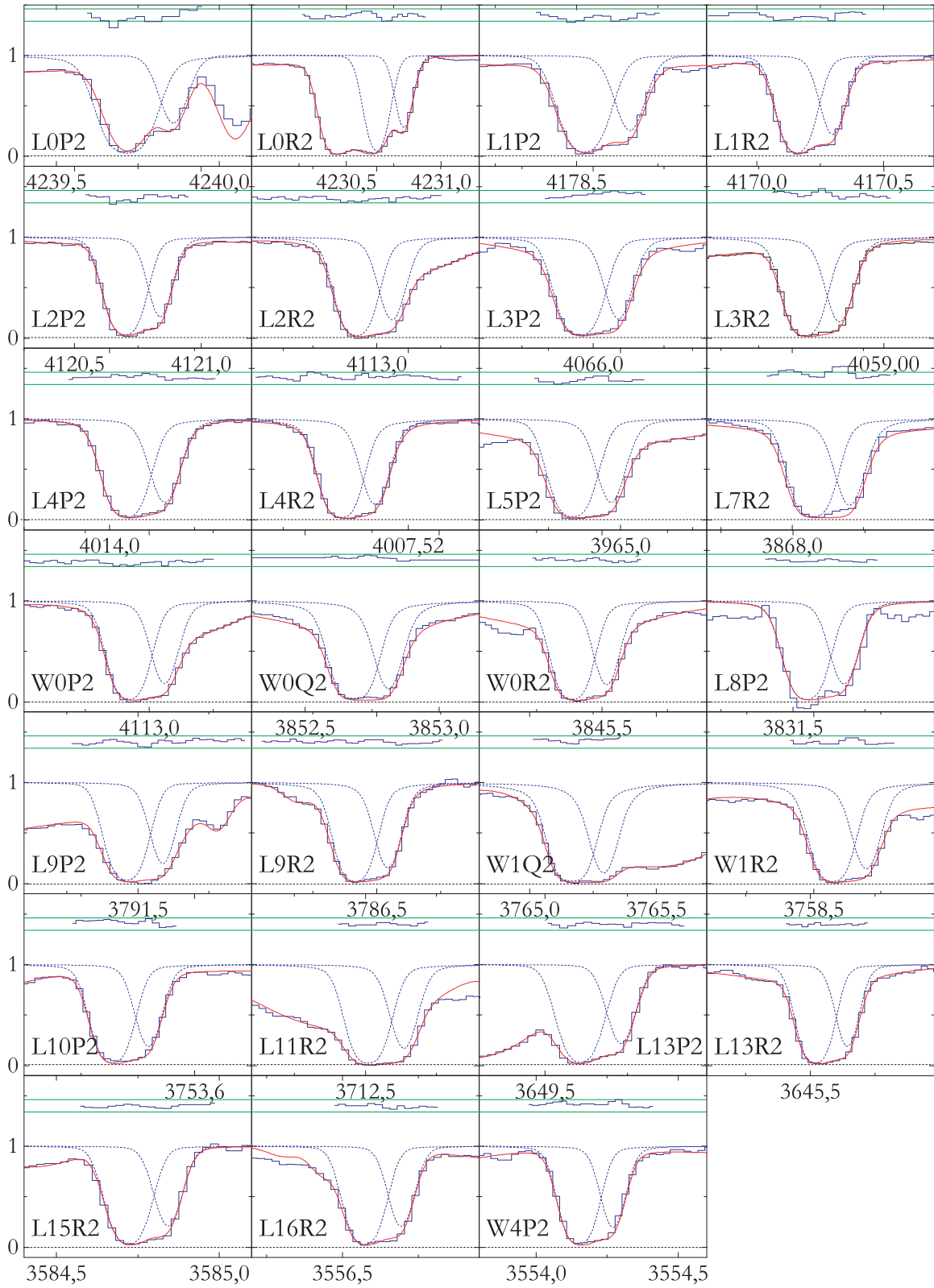


Figure C3. Best fit of the H₂ absorption lines from the $J = 2$ level at $z_{\text{abs}} = 2.811$ towards Q 0528–250. Colours and lines are the same as in Fig. C1.

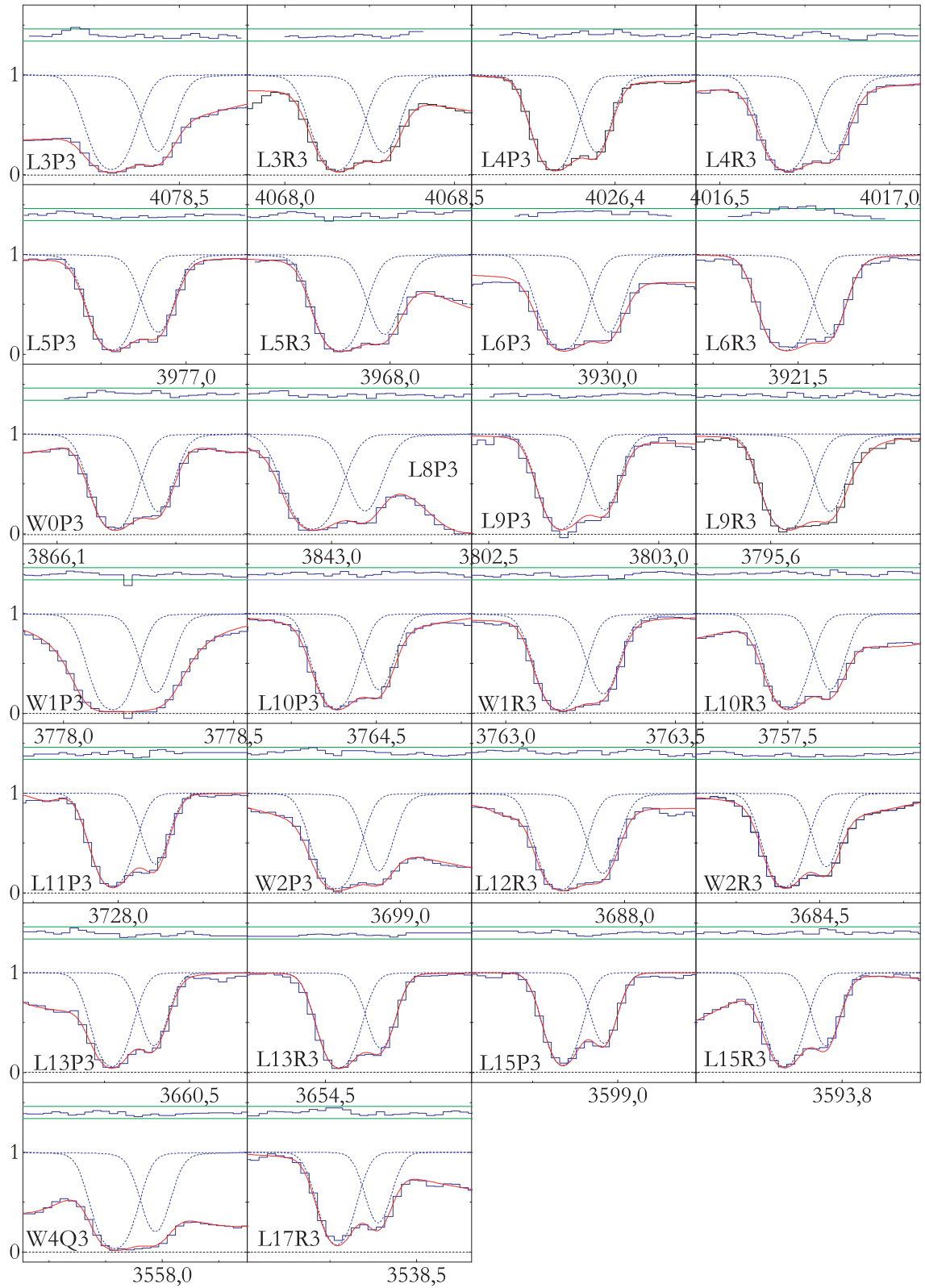


Figure C4. Best fit of the H₂ absorption lines from the $J = 3$ level at $z_{\text{abs}} = 2.811$ towards Q 0528–250. Colours and lines are the same as in Fig. C1.

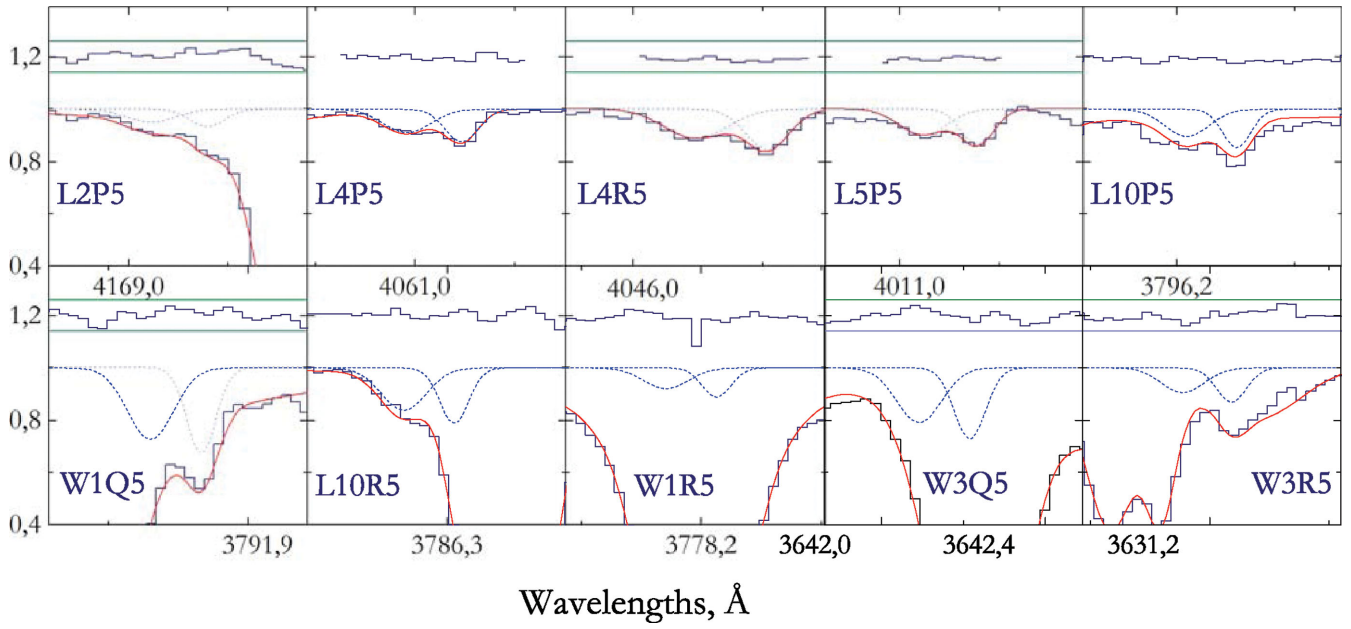


Figure C5. Best fit of the H₂ absorption lines from the $J = 5$ level at $z_{\text{abs}} = 2.811$ towards Q 0528–250. Colours and lines are the same as in Fig. C1.

Downloaded from https://academic.oup.com/mnras/article/448/1/280/990571 by CNRS - ISTO user on 25 April 2022

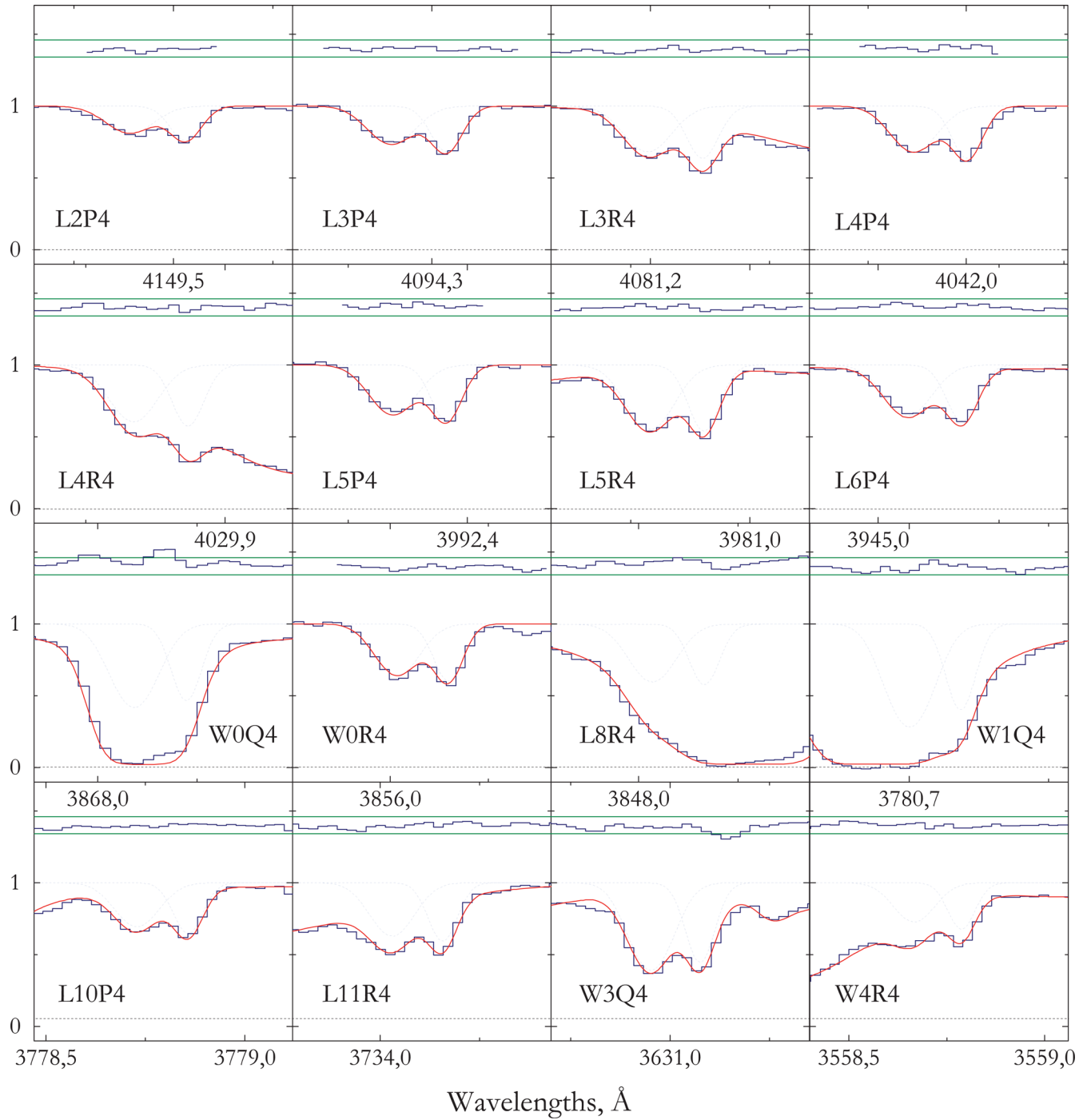


Figure C6. Best fit of the H₂ absorption lines from the $J = 4$ level at $z_{\text{abs}} = 2.811$ towards Q 0528–250. Colours and lines are the same as in Fig. C1.

This paper has been typeset from a $\text{\TeX}/\text{\LaTeX}$ file prepared by the author.